Experimental and modeling study on the thermal response of vertical storage tanks with different filling levels

Xiaoyang Yu[1,2], Jinwen Bai[1], Chenyu Zhu[1] , Ruowen Zong[1,2*]
1.State Key Laboratory of Fire Science, University of Science and Technology of China Hefei, Anhui, 230026, China

2. Suzhou Key Laboratory of Urban Public Safety, Suzhou Institute for Advanced Study, University of Science and Technology of China, Suzhou, Jiangsu 215123, China

Abstract

When liquid storage tanks are accidentally exposed to fire, they may explode due to rising internal pressure and structural deformation. To better understand failure mechanisms, this study examines the thermal response of externally heated tanks. Through combined experimental and computational analysis, we investigated thermal behaviors at various fill levels. Notably, temperature distributions in both the stored medium and tank walls, along with pressure responses, exhibited distinct patterns depending on fill levels. Our findings reveal that heated tanks experience rapid liquid temperature stratification, with thermal stratification intensity increasing proportionally to fill level. Interestingly, while pressure and evaporation rates at the vapor-liquid interface rose with fill level, wall temperature changes demonstrated an inverse relationship. Considering that both high temperature and high pressure could lead to a tank failure, a functional relationship between the probability of tank failure and filling levels has been established to reveal the combined effect of the wall temperature and pressure.

Keywords: vertical storage tank; filling levels; thermal response; thermal stratification; tank failure

1 Introduction

Large-scale water tanks are widely used for energy storage and thermal management in engineering applications such as nuclear power plants, solar energy systems, and chemical industry cooling systems[1-3]. In nuclear facilities, the containment-refueling water tank—equipped with an internal heat exchanger—acts as a key component of the passive waste-heat removal system. This system safely and continuously dissipates core decay heat without

Correspondence to: zongrw@ustc.edu.cn

requiring external intervention[4]. The thermal dissipation capacity of a tank is therefore critical to ensuring nuclear plant safety. Its thermal performance depends on complex thermal-hydraulic phenomena, which stem from flow characteristics shaped by external mass and heat inputs[5-8]. A thorough understanding of these thermal response patterns is essential for optimizing tank design and operation.

Prior research has examined the factors that contribute to the ruptures of tanks that contain various liquids. These factors include elevated wall temperatures, increases in the temperature of the contained medium, and the consequent rise in internal pressure. Based on experiments [9-13] and numerical simulations [14-17], researchers have investigated the response process of the above factors when the tank is exposed to heat. When the tank is heated from the outside, the temperature of the liquid near the wall rises rapidly, causing the liquid to become light and rise to the liquid surface due to buoyancy effects. This leads to a drop in the liquid temperature from top to bottom, which is known as liquid thermal stratification. The formation of liquid thermal stratification can be more intuitively observed in the experiments of Das et al. [18], where the fluorescent dye was injected into the heated liquid to achieve flow visualization. Previous works indicate that the internal vapor pressure is dictated by the temperature of the top liquid [19-21]. Thus, one must take into account the effects of liquid thermal stratification when calculating the internal pressure by using numerical models[22]. Thermal stratification occurs not only in the liquid space but also in the vapor space. A significant temperature stratification in the vapor space was found in the experiments of Heymes et al. [23], where the tank with a low filling level was exposed to th heat. Ren et al. [24] found that there was almost no thermal stratification in the vapor space at the early stage of heating, while the phenomenon of thermal stratification gradually became obvious after a period. In addition, the wall was also thermally stratified due to the effect of liquid and vapor thermal stratification [24]. In summary, the thermal stratification of the tank includes liquid thermal stratification, vapor thermal stratification and wall thermal stratification. The thermal stratification results in a continuous heat transfer from the high-temperature area to the low-temperature area, which greatly affects the temperature and pressure response. The mechanical strength of the tank wall starts to decrease as the wall temperature exceeds a certain value; in contrast, the internal pressure increases as the temperature of the liquid and vapor rises. If the stress induced in the tank wall due to the internal pressure is greater than the mechanical strength of the tank wall, the tank wall will deform and thus fail [25]. Therefore, tank failure is closely related to the thermal

response, including the temperature and pressure response [26].

The thermal response of liquid storage tanks is a complex multifactor coupling process involving solid-vapor heat transfer, solid–liquid heat transfer, vapor-liquid heat transfer and vapor-liquid phase transition, which depends on many factors, including the received heat flux, tank geometry, PRV set pressure and filling levels [23]. Previous works have comprehensively investigated the impact of the first three factors on the thermal response under a single filling level [16, 19, 23]. However, there is still little systemic experimental work to investigate the influence of different filling levels on the thermal response.

In this paper, a series of experiments with different filling levels were conducted to obtain the temperature distribution of the tank wall and medium, as well as the pressure response. The development of thermal stratification and its influence on the temperature response have been discussed under different filling levels. From the perspective of tank failure, the variation in the pressure and wall temperature with the filling level was analyzed. Finally, one function of the tank failure probability is proposed by balancing the effects of the wall temperature and pressure.

2 Experiment and numerical simulation description

2.1 Experimental procedure

In an indoor space, the experiment was carried out based on a small-scale tank, as shown in Fig. 1(a). The geometric parameters of the tank are listed in Table 1.

Table 1 Geometric parameters of the tank

Volume	Inner diameter	Outer diameter	The height of main body (H)
60 L	330 mm	350 mm	700 mm

To study the response process of the tank with different filling levels, experiments of four liquid heights were conducted. Four liquid heights h (140 mm, 245 mm, 350 mm and 455 mm) correspond to four different filling levels f (20%, 35%, 50% and 65%).

As illustrated in Fig. 1 (b), six K-type thermocouples are arranged vertically along the central axis to measure the medium temperature inside the tank. The holes on the tank wall were sealed with high-temperature glue to ensure airtightness during the heating process. Taking the filling level f=50% (see エラー! 参照元が見つかりません。b) as an example, the thermocouples from bottom to top are T_{L1}, T_{L2}, T_{L3}, T_{L4}, T_{V1} and T_{V2} (subscript L represents liquid, subscript V represents vapor, and subscripts 1~6 increase from bottom to top). The

spacing of these thermocouples was 105 mm, ensuring that there was always one thermocouple located at the liquid-vapor interface under different filling levels (such as T_{L4} in Fig. 1b). This special thermocouple was used to measure the liquid surface temperature.

The tank wall temperature was monitored by six K-type thermocouples fixed to the external surface of the tank. As shown in エラー! 参照元が見つかりません。b, the thermocouples from bottom to top are T_{WL1}, T_{WL2}, T_{WL3}, T_{WL4}, T_{WV1} and T_{WV2} (subscript WL represents the wet wall in contact with liquid, subscript WV represents the dry wall in contact with vapor). The height of the external thermocouples is consistent with that of the internal thermocouples.

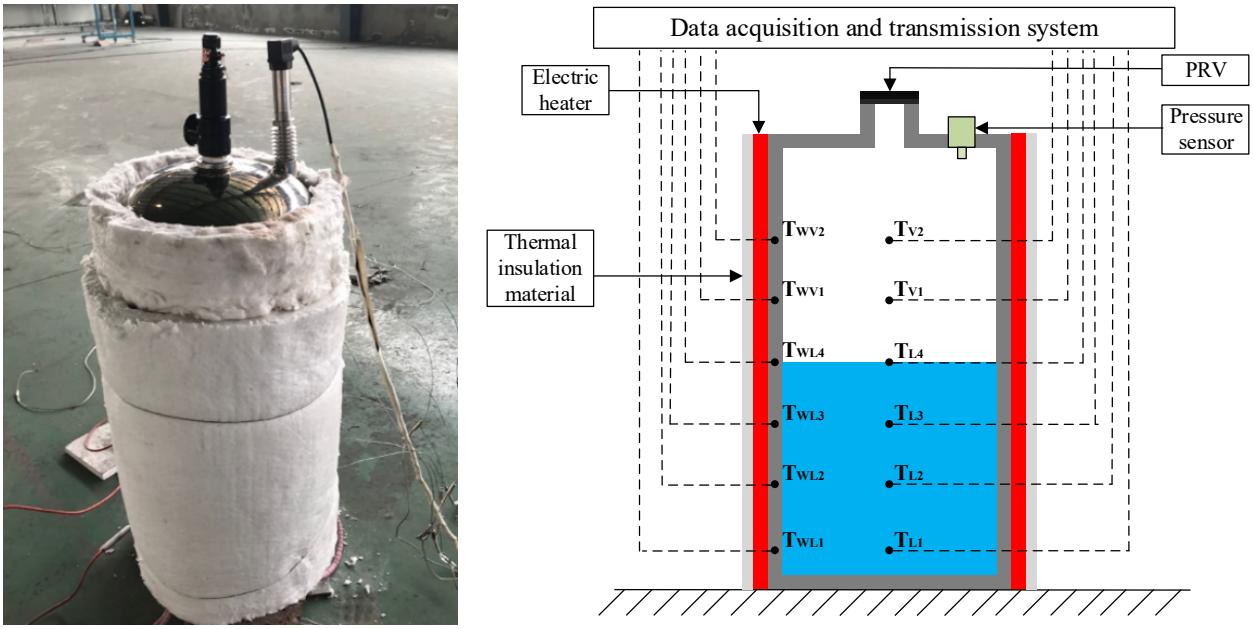

(a) (b)

Fig. 1 The experimental equipment. (a) Small-scale tank. (b) Schematic diagram.

Water was used as the filling medium in this experiment, and water was successfully used to investigate the temperature and pressure response of the tank [24, 27]. The distance between the flame and tank, the wind speed and other factors affect the radiant flux received by the tank wall, which makes the calculation of radiation extremely complicated. Therefore, a simplified method was used to simulate the flame radiation at a certain distance by using an electric heater wrapping around the tank (see Fig. 1), which kept the heat flux received by the tank wall uniform and constant [22]. The actual output power of the electric heater was 8 kW, and the heat flux was 10 kW/m^2. In addition, the white ceramic fiber blanket (thermal insulation material) wrapped around the electric heater reduced the heat loss and improved the heating

efficiency.

A PRV (pressure relief valve) and a pressure sensor (see Fig. 1) with a range of 0~4 MPa were installed at the top of the water tank, which was externally connected with a 24 V stabilized DC power. The thermocouples and pressure sensors were connected to the computer via an Agilent 34972A data acquisition and transmission system, which was used to obtain and store data in real time.

2.2 Numerical model

The thermal response behavior of the tank is the result of the coupling of processes including heat conduction within the tank wall, interphase mass transfer, and convection. In this work, we established a thermal mass coupling calculation model based on the computational fluid dynamics method to analyze the characteristics of temperature stratification and evaporation at the vapor-liquid interface in tanks with different filling levels.

The model was implemented by ANSYS Fluent 2021. The volume of fluid (VOF) was selected as a multiphase model, which is suitable for simulating a system featuring two or more immiscible phases. The transport equations for mass, momentum, turbulence (k-ω SST model) and energy are reported in Table 2. The specific discretization schemes are shown in Table 3.

Table 2 Governing equations implemented in the CFD model

ID	Equation	Description
E01	$\frac{\partial}{\partial t}(\alpha_l \rho_l) + \nabla \bullet (\alpha_l \rho_l \vec{u}) = \dot{m}_{vl} - \dot{m}_{lv}$	ρ_l : liquid density; t : time; α_l : liquid volume fraction; $\vec{u}$: Reynolds averaged velocity; $\dot{m}_{lv}$ and $\dot{m}_{vl}$: evaporation and condensation liquid phase source terms
E02	$\alpha_V = 1 - \alpha_L$	α_V : vapor volume fraction
E03	$\rho = \rho_l \alpha_l + \rho_V \alpha_V$	ρ : two-phase volume fraction averaged density; α_V : vapor volume fraction; ρ_V : vapor density
E04	$\frac{\partial}{\partial t}(\rho \vec{u}) + \nabla \bullet (\rho \vec{u} \vec{u}) = -\nabla p + \nabla \bullet \bar{\bar{\tau}} + \rho \vec{g}$	p : Reynolds averaged pressure; $\bar{\bar{\tau}}$: stress tensor
E05	$\frac{\partial}{\partial t}(\rho E) + \nabla \bullet [\vec{u}(\rho E + p)] = \nabla \bullet (k \nabla T) + S$	E : two-phase averaged specific energy; k : thermal conductivity; S : Energy source item

E06	$E = \frac{\alpha_l \rho_l E_l + \alpha_v \rho_v E_v}{\alpha_l \rho_l + \alpha_v \rho_v}$	E_l : liquid specific energy; E_v : vapor specific energy

Table 3 Specific discretization schemes in Fluent

Item	Description
Boundary conditions	constant heat flux （10 kw/m^2）
Mathematical models	Continuity: VOF (Volume of Fluid) method Turbulent Flow: SST k-ω Model
Transient Pressure-Velocity coupling algorithm	SIMPLEC
Spatial discretization scheme	PRESTO! for pressure; Least Square Cell-Based for gradient; first order discretization scheme in all other cases
Primary phase for VOF	Vapor phase
Patched variable for VOF	Liquid phase volume fraction
Convergence criteria	10^{-6} for all the equations
Type of mesh	Tetrahedrons
Time step (s)	0.01

Interphase mass transfer can be achieved through an evaporation-condensation model (Lee model) in Fluent. The fluid medium was water, and the heat flux of the sidewall was 10 kw/m^2. The vapor phase density was calculated using the ideal gas equation. The tank model is shown in Fig. 2, the number of cells was 504398, and a grid independence study was successfully performed to generate a finer mesh featuring 3654905.

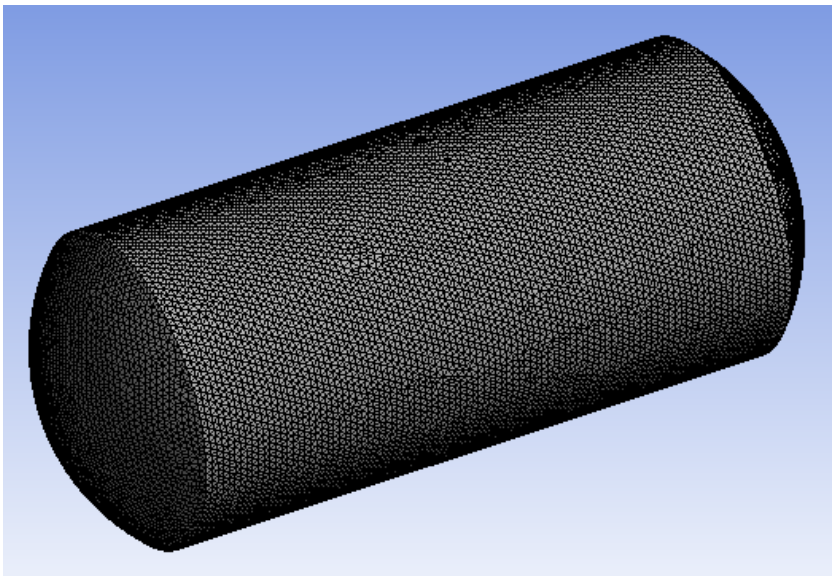

Fig. 2 Grid model of the vertical storage tank

Fig. 3 shows the comparison of the experimental and simulation results at a filling level of 35%. The simulation measurement location is consistent with the experimental measurement point arrangement. The vapor and liquid temperatures are slightly incompatible, but the error is within the allowable range. Therefore, numerical models can be used to evaluate the thermal response behavior of storage tanks.

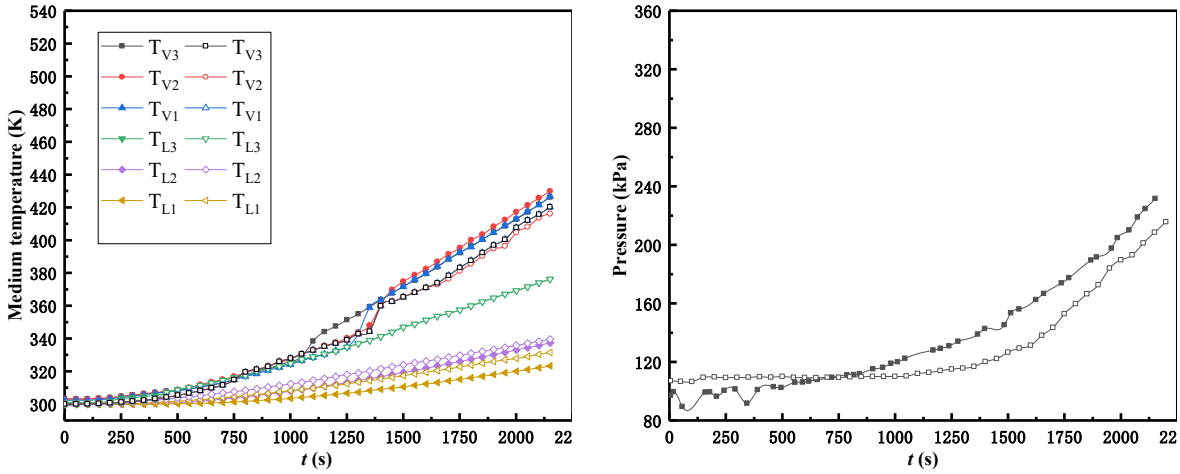

(a) (b)

Fig. 3 Comparison of experimental and simulation results at *f*=35% (Solid symbols indicate experimental results, hollow symbols indicate simulation results): (a) medium temperature, (b) pressure.

3 Results and discussion

3.1 The temperature response of the medium

Fig. 4 illustrates the temperature response of the medium under various filling levels, with

TL2, TL3, TL4, and TL5 representing the liquid surface temperatures for each respective level. Notably, the medium temperature remains nearly constant prior to 250 s. Given the tank wall thickness of 20 mm, radial heat conduction is non-negligible. Prior to 250 s, the heat absorbed by the tank is predominantly used for conduction between the outer and inner walls, while convective heat transfer between the inner wall and the medium remains limited. This results in a nearly constant medium temperature. After 250 s, convective heat transfer gradually strengthens, and a thermal boundary layer forms near the inner wall. The heated liquid within this layer rises due to buoyancy effects, driving natural convective heat transfer. Upon reaching the liquid surface, the warm fluid flows toward the low-temperature region at the surface center, thereby heating the colder liquid beneath. This process facilitates the development of a temperature stratification layer. As heating progresses, the temperature difference within the stratification layer becomes increasingly pronounced, indicating enhanced thermal stratification of the liquid (see Fig. 4).

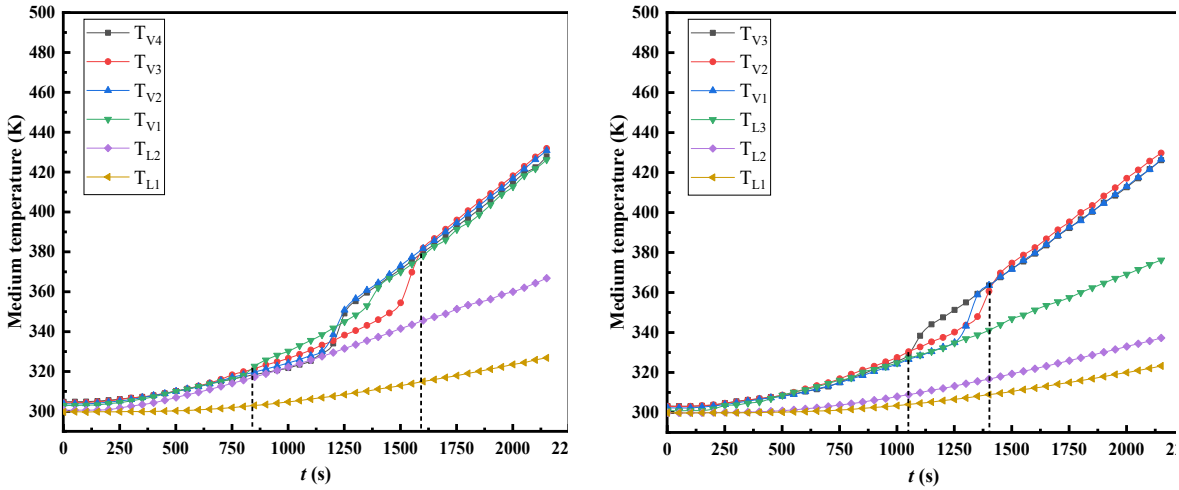

(a) (b)

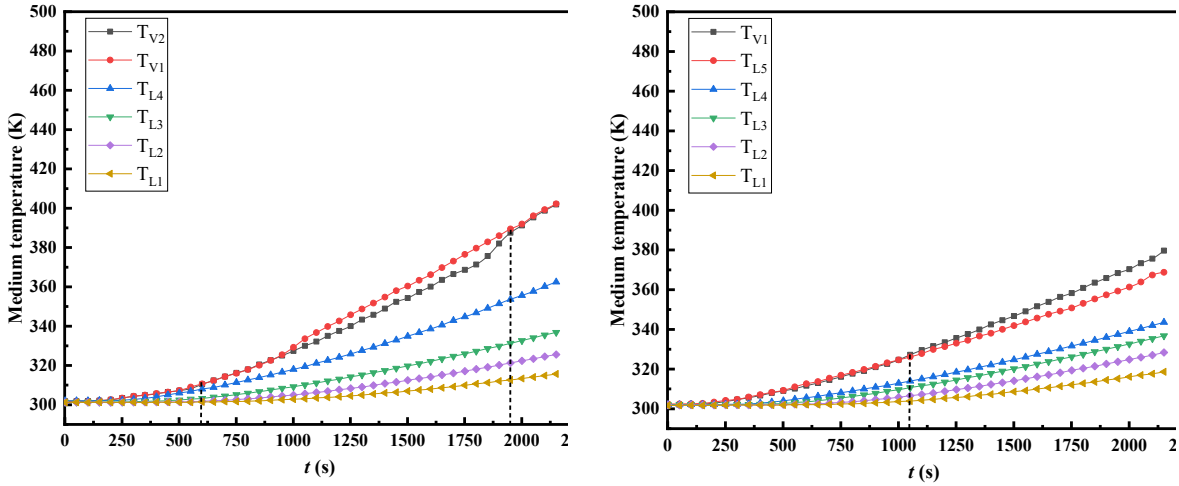

(c) (d)

Fig. 4 Temperature response of the medium under different filling levels: (a) f=20%, (b) f=35%, (c) f=50% and (d) f=65%.

The degree of liquid thermal stratification is governed by the temperature gradient from bottom to top in the liquid space. The temperature gradient can be calculated by:

$$\bar{k} = \frac{\sum_{i=1}^{N-1} \frac{R_{L(i+1)} - R_{Li}}{\Delta x}}{N-1} \tag{1}$$

Here, $\bar{k}$ is the average temperature gradient, K/m; R_{Li} is the temperature monitored by the thermocouple T_{Li}, K; Δx is the spacing of the thermocouples, Δx = 0.105 m; and N is the number of thermocouples in the liquid space, which depends on the filling levels. Based on the experimental data in エラー! 参照元が見つかりません。4, the temperature gradient in the liquid space can be calculated by equation (1).

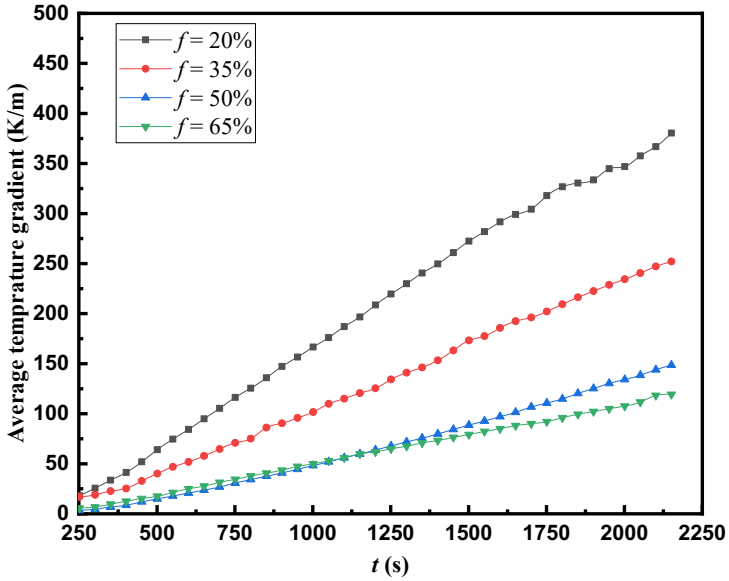

Fig. 5 The average temperature gradient in the liquid space with different filling levels.

It can be seen from Fig. 5 that the average temperature gradient increases linearly with the heating time and the rising rate or slope decreases with the filling level. At the same time, the value of $\overline{k}$ always declines with the filling level, meaning that the degree of liquid thermal stratification decreases with the filling level. Fig. 6 illustrates the temperature distribution characteristics in the flow field at various filling levels after 2000 s of heating. The extent of thermal stratification becomes more pronounced at lower filling levels. Enhanced natural convection intensity improves fluid mixing, leading to reduced temperature gradients within the liquid region (Ren et al., 2017). This demonstrates that natural convection intensifies proportionally with filling level. Notably, the disparity between adjacent curves decreases with higher filling levels, particularly between the f=50% and f=65% cases. These observations indicate that the influence of filling levels on thermal stratification diminishes as the filling level increases.

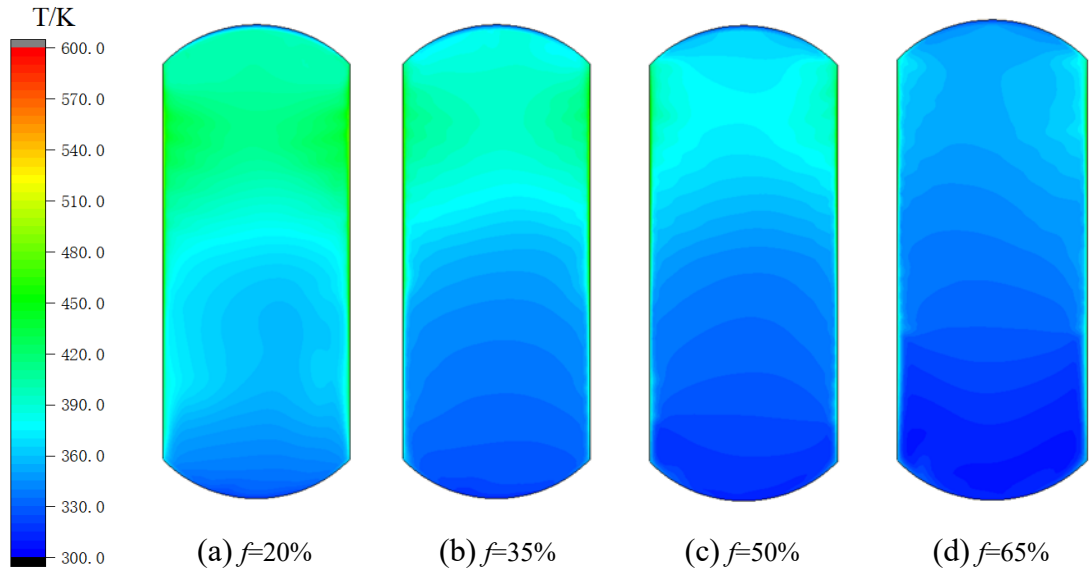

Fig. 6 Temperature distribution characteristics of the flow field at different filling levels when heated for 2000 s

As shown in Fig. 4(a)-(c), vapor thermal stratification emerges exclusively during the mid-phase heating period (see vertical dotted markers). Using the f=20% case as an example, the vapor temperature profile remains largely uniform and consistent with the liquid surface temperature prior to 870 s. This equilibrium state, maintained via evaporation-condensation processes, demonstrates thermodynamic coupling between the vapor phase and liquid surface. Beyond 870 s, the vapor enters a superheated state exceeding the pressure-dependent saturation temperature. During the 870-1600 s interval, non-uniform superheat distribution establishes thermal stratification within the vapor space. However, intense molecular motion subsequently induces turbulent homogenization. Therefore, after 1600 s, the vapor temperature is uniform again, and the thermal stratification starts to disappear, which is called destratification.

Fig. 7 shows the internal fluid temperature stratification phenomenon at f=20%. During heating, heat conduction first occurs within the storage tank, followed by convective heat transfer between the tank wall and the fluid medium. As heating progresses, the temperature of the fluid adjacent to the wall increases while its density decreases, forming a thermal boundary layer. The heated boundary layer liquid rises due to buoyancy effects, initiating natural convective heat transfer. When the warm liquid reaches the liquid surface, it spreads toward the low-temperature region at the surface center, transferring heat to the colder liquid below. As the fluid temperature approaches saturation temperature, boiling initiates at the fluid boundary with bubble formation, significantly enhancing heat transfer efficiency. Concurrently, the evaporation rate at the liquid-vapor interface increases, causing the gradual disappearance of

vapor temperature stratification until a uniform temperature distribution is achieved.

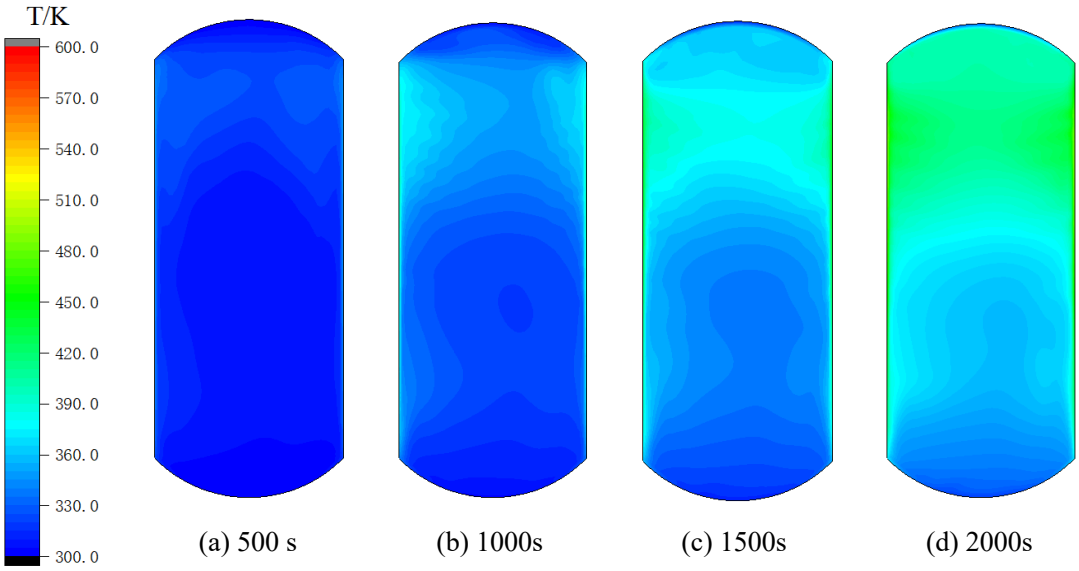

Fig. 7 Medium temperature clouds in the storage tank at different moments at f=20%

The temperature rise rate of the medium under different filling levels is presented in Fig. 8. Throughout the heating process, the vapor’ s temperature rise rate consistently exceeds that of the liquid due to its lower specific heat capacity. After the initial heating phase, the fluctuation range of the vapor’ s temperature rise rate becomes greater than that of the liquid, as the vapor reaches a superheated state, leading to a more unstable increase rate. Fig. 8 demonstrates that the temperature rise rate in the liquid space gradually rises from bottom to top. The warmer liquid accumulates at the top of the liquid space and transfers heat to the cooler liquid below, resulting in a higher temperature rise rate near the top. In Fig. 8(a) and (b), several abrupt fluctuations are observed in the vapor space. However, these fluctuations are absent at higher filling levels (see Fig. 8(c) and (d)), indicating that they diminish as the filling level increases. During the experiments, residual air was present in the liquid storage tank. Lower filling levels correspond to a greater volume of residual air, which suggests that higher air content induces pronounced fluctuations in the temperature rise rate. This phenomenon is closely linked to the degree of superheating in the gas phase, as air undergoes superheating more readily than water vapor. Consequently, residual air in the tank elevates the risk of structural failure when the tank is subjected to heat radiation.

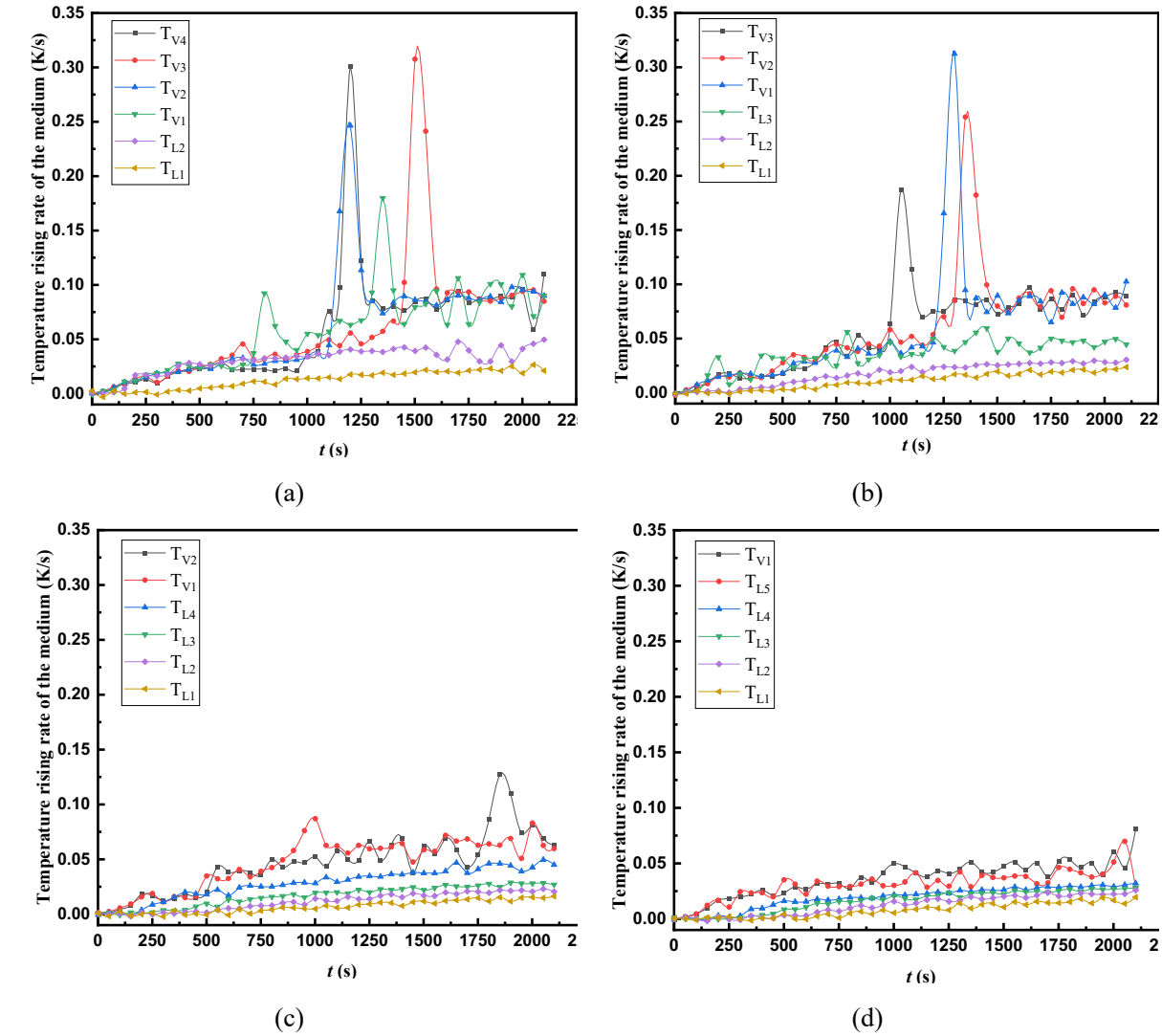

Fig. 8 Temperature rising rate of the medium under different filling levels: (a) f=20%, (b) f=35%, (c) f=50% and (d) f=65%.

The rate of temperature increase of the medium is negatively correlated with the heat absorption capacity of the medium. Fig. 8 shows that the overall rate of temperature increase decreases with the filling level, which indicates that the overall heat absorption capacity of the medium increases with the filling level.

3.2 Temperature response of the tank wall

The temperature response of the tank wall under different fill levels is shown in Fig. 9, where TWL2-TWL5 denote the interface temperatures between the dry and wet walls. The dry wall consistently exhibits higher temperatures than the wet wall due to the liquid's enhanced cooling capacity, attributable to its greater specific heat capacity and higher heat transfer coefficient. This drives a continuous vertical heat conduction process from the dry to the wet

wall. Liquid thermal stratification significantly influences the wet wall's temperature distribution, inducing stratified temperature patterns in the tank wall (Fig. 9). In contrast, the dry wall shows no discernible thermal stratification, behavior consistent with the vapor phase characteristics. These findings demonstrate that the tank wall's thermal response is predominantly governed by the medium contacting its interior surface. Increased fill levels intensify cooling at the dry-wet wall interface, resulting in temperature reduction at this boundary. While the interface temperature closely matches the dry wall temperature in Fig. 9(a) and (b), a pronounced temperature differential emerges in Fig. 9(c) and (d). This indicates an abrupt enhancement in liquid-mediated interface cooling when fill levels increase from 35% to 50%.

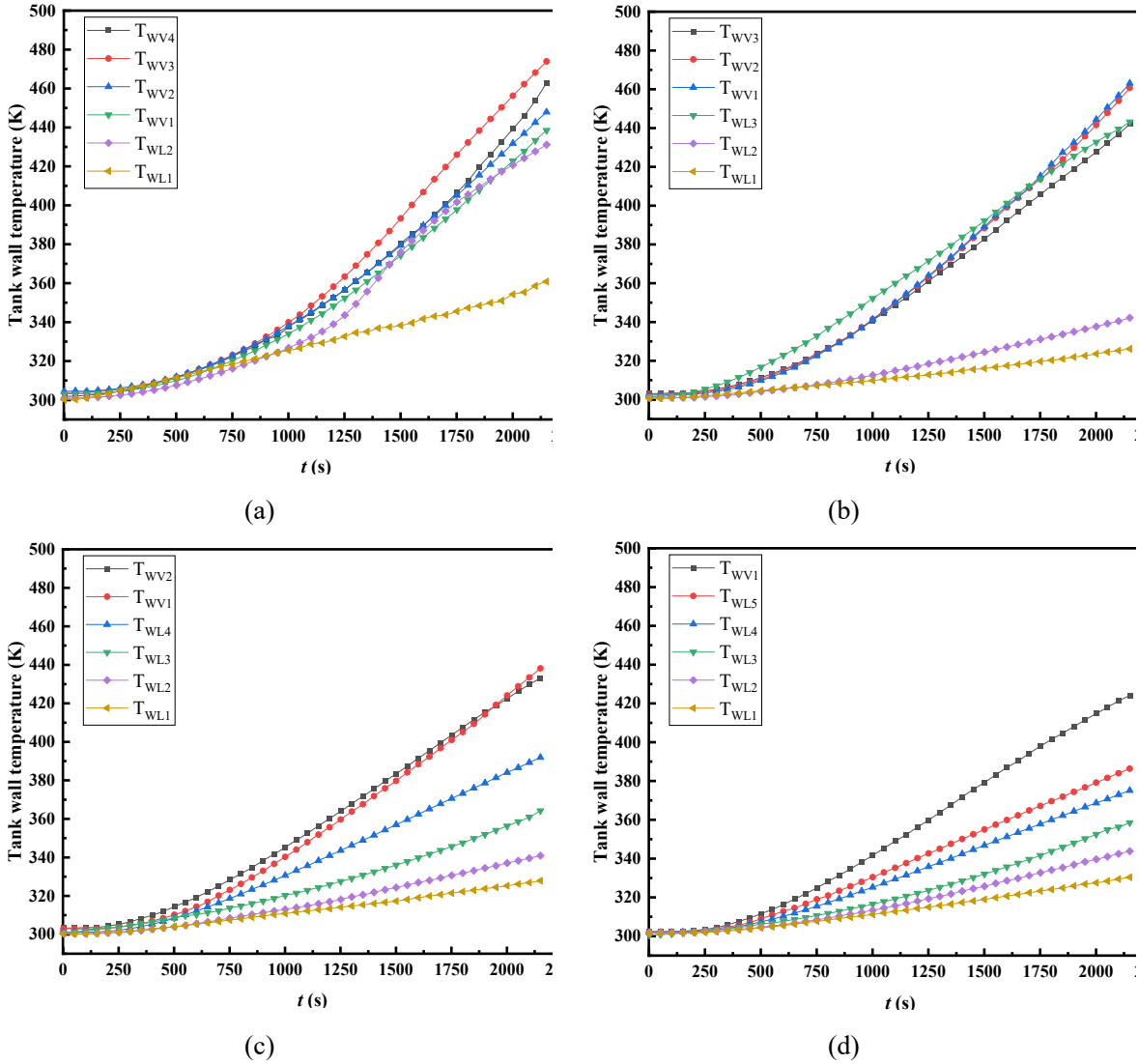

Fig. 9 Temperature response of the tank wall under different filling levels: (a) *f*=20%, (b) *f*=35%, (c)

***f*=50% and (d) *f*=65%.**

The temperatures monitored by the six thermocouples are averaged to represent the average wall temperature, as shown in Fig. 10. At the middle and later stages of heating, the average tank wall temperature decreases with the filling level. Similarly, the maximum wall temperature selected from Fig. 10 decreases with the filling level in Fig. 11. It is worth noting that the average wall temperature or maximum wall temperature exhibits the largest drop as the filling level increases from 35% to 50%. This indicates that the filling level between 35% and 50% has the largest influence on the wall temperature.

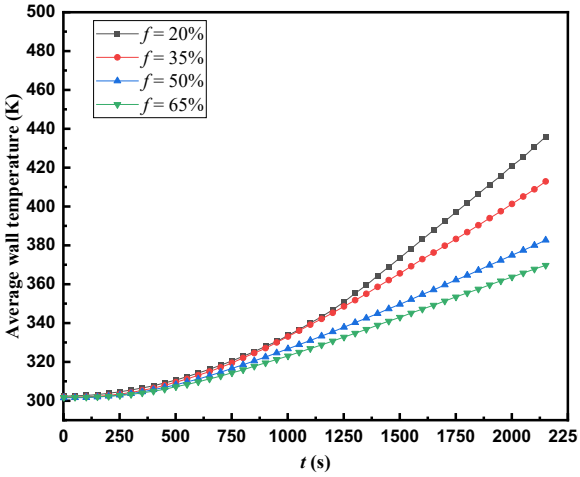

Fig. 10 The average wall temperature.

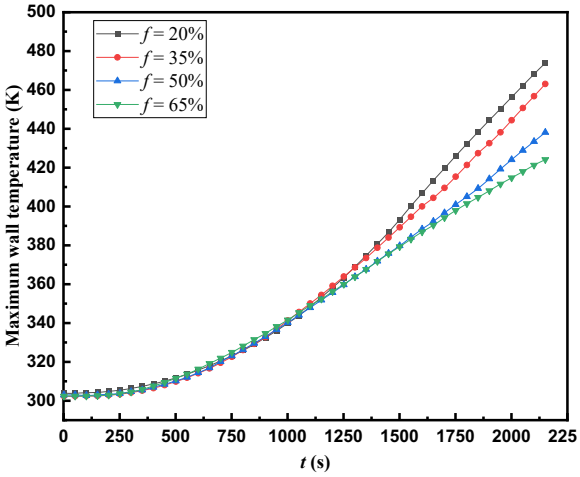

Fig. 11 The maximum wall temperature.

3.3 Hazard analysis of the tank

Fig. 12 illustrates the pressure response in a tank subjected to constant heat flux. Prior to 250 s, the pressure remains at its initial value because the temperature of the governing medium (which determines the pressure) also remains unchanged (see Fig. 4). Until 1400 s, the pressure response curves for different filling levels nearly coincide, indicating minimal influence of filling level on pressure. Beyond 1400 s, however, the curves begin to diverge significantly, with pressure increasing proportionally to filling level. During this stage, the vapor temperature exceeds the saturation temperature corresponding to the liquid surface, reaching a superheated state that intensifies thermal motion. Crucially, tanks with higher filling levels have smaller gas spaces. Since the liquid surface temperatures are similar across filling levels (Fig. 12), the mass of water vapor entering the gas space through phase change is nearly identical. This results in a greater pressure increase within smaller gas volumes. The interplay of these factors drives the observed correlation between pressure and filling level during the later heating phase.

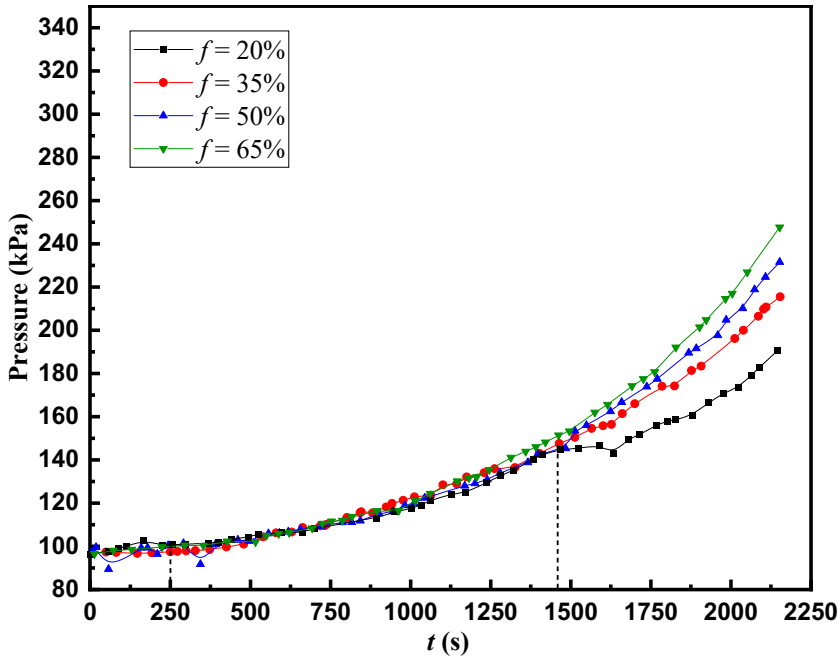

Fig. 12 The pressure response under different filling levels.

The pressures from 1400 s to 2150 s in Fig. 12 are averaged as $\overline{P}$. Similarly, the temperatures from 1400 s to 2150 s in Fig. 11 are averaged as $\overline{T}$. The average value of pressure and wall temperature from 1400 s to 2150 s are shown in Fig. 13. The rising rate of $\overline{P}$ decreases with the filling level, and the declining rate of $\overline{T}$ decreases with the filling level, which indicates that the effects of the filling level on $\overline{P}$ and $\overline{T}$ are weakened as the filling level increases.

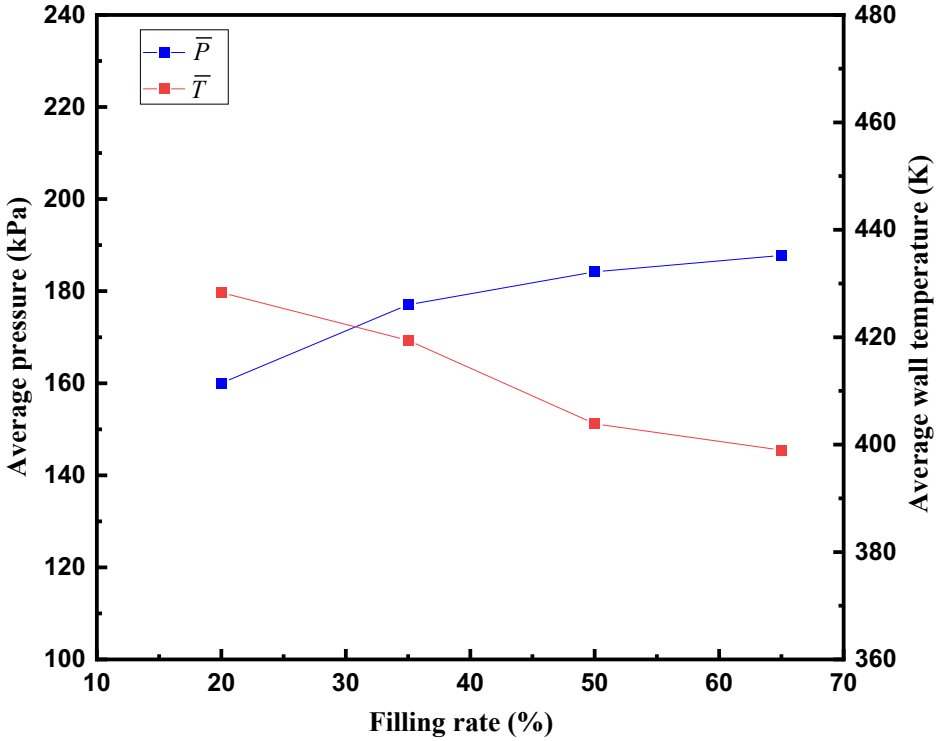

Fig. 13 The average pressure and wall temperature from 1400 s to 2150 s.

To prevent the tank from being exposed to fire impingement and breaking, it is crucial to reduce both the maximum wall temperature and internal pressure. Elevated wall temperatures weaken the tank wall material strength (Birk, 1990) or cause failure in pressure fittings constructed from low-melting-temperature metals (Heymes et al., 2013). Simultaneously, increased pressure exerts additional stress on the inner wall. When this stress exceeds the material's strength limit, tank failure occurs. In this study, the wall temperature and internal pressure exhibit inversely correlated trends as fill level increases (Fig. 13). Higher fill levels correspond to greater liquid volume, which enhances wall cooling and lowers temperature. Conversely, reduced gas space at higher fill levels elevates pressure. Therefore, determining an optimal fill level requires balancing these competing thermal and mechanical effects.

The functional relationship between the yield strength of the steel and the wall temperature has been given by the following equation:

$$\sigma_s(T(f)) = \begin{cases} \sigma \cdot (1 + \dfrac{T(f)}{767 \ln(T(f)/1750)}) & 0 \le T(f) \le 600 \quad (1) \\ 108\sigma \cdot (\dfrac{1 - T(f)/1000}{T(f) - 440}) & T(f) > 600 \quad (2) \end{cases}$$

Here, f is the filling level. $\sigma_s(T(f))$ is the yield strength as a function of the wall temperature

$T(f)$, MPa. σ is a constant value, MPa. $T(f)$ is the wall temperature, ℃. $\sigma_s(T(f))$ is a decreasing function of $T(f)$, and $T(f)$ is a decreasing function of f. This means that $\sigma_s(T(f))$ is an increasing function of f.

A fissure usually forms in the dry wall because the yield strength of the dry wall is lower due to the higher wall temperature (see Fig. 9). Tank failure with mechanical rupture will occur on the dry wall if the equivalent stress reaches the yield strength [28]. The equivalent stress is calculated by the internal pressure, and the thermal stress is induced by the differential temperature on the dry wall [29]. There is no obvious temperature difference on the dry wall (see Fig. 9), so the thermal stress can be neglected. Thus, the equivalent stress $P(f)$ is approximately equal to the stress load generated by the internal pressure. The internal pressure increases with the filling level, so the equivalent stress $P(f)$ is an increasing function of f. Then, the functional relationship between the probability of tank failure $F(f)$ and filling level is:

$$F(f) \propto \frac{1}{\sigma_s(T(f)) - P(f)} \tag{3}$$

$F(f)$ is inversely proportional to the value of $\sigma_s(T(f))$ minus $P(f)$. Equations (2) and (3) intuitively reveal the effect of the filling level on tank failure. Both high temperature and high pressure play an important role in promoting tank failure. The monotonicity of $\sigma_s(T(f))$ is the same as that of $P(f)$, so $F(f)$ may not be a monotonic function of f. It is likely that there is an extreme point f_m that makes the probability of tank failure reach the minimum. This paper cannot provide the exact expressions of $T(f)$ and $P(f)$ due to the limits of experiments. Further research is required to determine the exact expression of equation (3), including tank heating experiments with more filling levels.

4 Conclusion

A series of experiments and simulations were conducted to study the thermal stratification and response process of vertical storage tanks under external thermal aggression. The result could provide effective support for the failure analysis of liquid storage tanks. The temperature response of the medium and wall, as well as the pressure response, presents different characteristics under different filling levels. The main conclusions are as follows:

1) When the tank is under an external thermal attack, liquid thermal stratification occurs, and the degree of liquid thermal stratification increases linearly with the heating time. The degree of liquid thermal stratification decreases with filling levels, but the effect

of the filling level is severely weakened as the filling level exceeds 50%.

2) The vapor is superheated, and short vapor thermal stratification occurs. In the later stage of heating, the vapor thermal stratification disappears because the degree of superheat is uniform.

3) The rate of temperature increase of the vapor is always higher than that of the liquid. Obvious jumps in the rate of temperature increase occur in the vapor space but gradually disappear as the filling level increases. When the filling level is lower, more air is left inside the tank, resulting in obvious jumps in the rate of temperature increase.

4) The dry wall temperature is higher than the wet wall temperature due to the remarkable cooling effect caused by liquid. The wet wall temperature stratifies, but there is no obvious thermal stratification on the dry wall, which indicates that the temperature distribution of the wall is greatly affected by the medium with which the inside wall is in contact.

5) The average wall temperature decreases with the filling level, while the average pressure increases with the filling level, and the impact of the filling level is weakened as the filling level increases. Both high temperature and high pressure could cause the tank to fail, so the probability of tank failure is not a monotonic function of the filling level. There is an extreme point that makes the probability to reach the minimum.

Finally, one function of the tank failure probability is proposed by balancing the effects of the wall temperature and pressure. Further works can be applied to determine the exact functional relationship between the probability of tank failure and filling levels, which is helpful to determine an optimum filling level.

Acknowledgments

The work in this study was financially supported by the National Key Technology R&D Program (No.2023YFC3010201), Suzhou Science and Technology Plan Project (SYG2024060).

References

[1] Li Q., Huang X., Tai Y., Gao W., Wenxian L., Liu W., Thermal stratification in a solar hot water storage tank with mantle heat exchanger, Renewable Energy, 173 (2021) 1-11.

[2] Gomaa M.R., Murtadha T.K., Abu-jrai A., Rezk H., Altarawneh M.A., Marashli A., Experimental Investigation on Waste Heat Recovery from a Cement Factory to Enhance Thermoelectric Generation, Sustainability, 14 (2022).

[3] Tauveron N., Lhermet G., Payebien B., Caney N., Morin F., An Experimental Study of an Autonomous Heat Removal System Based on an Organic Rankine Cycle for an Advanced Nuclear Power Plant, Energies, 17 (2024).

[4] Kim M.J., Moon J.H., Bae Y., Kim Y.I., Lee H.J., Feasibility test of the concept of long-term passive cooling system of emergency cooldown tank, Annals of Nuclear Energy, 80 (2015) 403-408.

[5] Armstrong P., Ager D., Thompson I., McCulloch M., Domestic hot water storage: Balancing thermal and sanitary performance, Energy Policy, 68 (2014) 334-339.

[6] Gad H.E., Shet U.S.P., Gupta M.C., An experimental investigation on the thermal performance of a forced circulation solar water heating system, 3rd Miami International Conference on Alternative Energy Sources. Proceedings of Condensed Papers, (1980) 140-141.

[7] Bae H., Ryu S.U., Ryu H.B., Kim W.S., Yi S.J., Park H.S., Asme, An Experimental Investigation on Thermal-Hydraulic Interaction between Core Makeup Tank and Safety Injection Tank of an Integral Small Reactor during a Small Break Loss-of-Coolant Accident, in: Asme-Jsme-Ksme Joint Fluids Engineering Conference (AJK-FED), Seoul, South Korea, 2015.

[8] El-Morshedy S.E.-D., Thermal-hydraulic modeling and analysis of a tank in pool reactor for normal operation and loss of flow transient, Progress in Nuclear Energy, 61 (2012) 78-87.

[9] Stawczyk J., Experimental evaluation of LPG tank explosion hazards, Journal of Hazardous Materials, B96 (2003) 189-200.

[10] Tschirschwitz R., Krentel D., Kluge M., Askar E., Habib K., Kohlhoff H., Krüger S., Neumann P.P., Storm S.U., Rudolph M., Experimental investigation of consequences of LPG vehicle tank failure under fire conditions, Journal of Loss Prevention in the Process Industries, 56 (2018) 278-288.

[11] Ruban S., Heudier L., Jamois D., Proust C., Bustamante-Valencia L., Jallais S., Kremer-Knobloch K., Maugy C., Villalonga S., Fire risk on high-pressure full composite cylinders for automotive applications, International Journal of Hydrogen Energy, 37 (2012) 17630-17638.

[12] Birk A.M., Poirier D., Davison C., On the response of 500gal propane tanks to a 25% engulfing fire, Journal of Loss Prevention in the Process Industries, 19 (2006) 527-541.

[13] Manu C.C., Birk A.M., Kim I.Y., Stress rupture predictions of pressure vessels exposed to fully engulfing and local impingement accidental fire heat loads, Engineering Failure Analysis, 16 (2009) 1141-1152.

[14] Bi M.S., Ren J.J., Zhao B., Che W., Effect of fire engulfment on thermal response of LPG tanks, Journal of Hazardous Materials, 192 (2011) 874-879.

[15] Zheng J., Bie H., Xu P., Chen H., Liu P., Li X., Liu Y., Experimental and numerical studies on the bonfire test of high-pressure hydrogen storage vessels, International Journal of Hydrogen Energy, 35 (2010) 8191-8198.

[16] Landucci G., D'Aulisa A., Tugnoli A., Cozzani V., Birk A.M., Modeling heat transfer and pressure build-up in LPG vessels exposed to fires, International Journal of Thermal Sciences, 104 (2016) 228-244.

[17] Scarponi G.E., Landucci G., Heymes F., Cozzani V., Experimental and numerical study of the behavior of LPG tanks exposed to wildland fires, Process Safety and Environmental Protection, 114 (2018) 251-270.

[18] Das S.P., Chakraborty S., Dutta P., Studies on Thermal Stratification Phenomenon in LH2 Storage Vessel, Heat Transfer Engineering, 5 (2004) 54-66.

[19] Birk A.M., Cunningham M.H., Liquid temperature stratification and its effect on BLEVEs and their hazards, Journal of Hazardous Materials, 48 (1996) 219-237.

[20] Khurana T.K., Prasad B.V.S.S.S., Ramamurthi K., Murthy S.S., Thermal stratification in ribbed liquid hydrogen storage tanks, International Journal of Hydrogen Energy, 31 (2006) 2299-2309.

[21] Gursu S., Sherif S.A., Veziroglu T.N., Sheffield J.W., Analysis and Optimization of Thermal Stratification and Self-Pressurization Effects in Liquid Hydrogen Storage Systems—Part 2: Model Results and Conclusions, Journal of Energy Resources Technology, 115 (1993) 228-231.

[22] Gong Y.W., Lin W.S., Gu A.Z., Lu X.S., A simplified model to predict the thermal response of PLG and its influence on BLEVE, Journal of Hazardous Materials, A108 (2004) 21-26.

[23] Heymes F., Aprin L., Birk A.M., Slangen P., Jarry J.B., François H., Dusserre G., An experimental study of an LPG tank at low filling level heated by a remote wall fire, Journal of Loss Prevention in the Process Industries, 26 (2013) 1484-1491.

[24] Ren J., Zhang H., Yu J., Bi M., Sun S., Experimental research of heat-mass coupling response of liquid storage tanks, Journal of Hazardous Materials, 338 (2017) 502-507.

[25] Bubbico R., Mazzarotta B., Dynamic response of a tank containing liquefied gas under pressure exposed to a fire: A simplified model, Process Safety and Environmental Protection, 113 (2018) 242-254.

[26] Li Y., Jiang J., Zhang Q., Yu Y., Wang Z., Liu H., Shu C.M., Static and dynamic flame model effects on thermal buckling: Fixed-roof tanks adjacent to an ethanol pool-fire, Process Safety and Environmental Protection, 127 (2019) 23-35.

[27] Heymes F., Eyssette R., Lauret P., Hoorelbeke P., An experimental study of water BLEVE, Process Safety and Environmental Protection, 141 (2020) 49-60.

[28] Wang X., Zhou K., Mebarki A., Jiang J., Numerical Simulation of Thermal Response Behavior of Floating-roof Tanks Exposed to Pool Fire, Applied Thermal Engineering, 179 (2020) 115692.

[29] Birk A.M., Scale effects with fire exposure of pressure-liquefied gas tanks, Journal of Loss Prevention in the Process Industries, 8 (1995) 275-290.